Preparation of Solid-Supported Membrane Multilayers

Text S1: The solid-supported membrane multilayers were prepared by the deposition of a 0.5 mL portion of lipid mixtures dissolved in 7:3 mixtures (v/v) of $CHCl_3$ and CH_3OH at total concentrations of 2 mg/mL. To study the influence of the lateral density of Le^X groups at the membrane surface, we prepared lipid membranes that contained three different molar fractions of Le^X lipid (2 mol%, 10 mol%, and 25 mol% Le^X lipid) and pure d-DPPC membranes (control). Prior to the membrane deposition, we cut Si(100) substrates with native oxide (Si-Mat, Landsberg/Lech, Germany) into rectangular shapes (55 mm x 25 mm) and cleaned them by a modified RCA method(1). The wafers were stored at 70 °C for 3 h, and subsequently in a vacuum chamber overnight to remove the residual solvent. The average number of membranes in the stacks could be roughly estimated to be in the order of several hundred from the amount of solution and the coated area. The samples were hydrated and annealed at least twice by heating/cooling between 20 °C and 70 °C at a high relative humidity ($h_{rel} > 95$ %). To cancel the thermal history of the samples, they were stored at 4 °C overnight prior to the measurements. Since all the lipids used in this study possess perdeuterated hydrocarbon chains, the samples were immersed into H_2O buffers (MilliQ, Molsheim, France) during the scattering experiments to achieve the maximum contrast in scattering length density between hydrated region and hydrocarbon chains.

(1) Kern, W., and D. A. Puotinen. 1970. Cleaning solutions based on hydrogen peroxide for use in silicon semiconductor technology. RCA Rev. 31:187.

Mechanical Parameters of Interacting DPPC Membranes

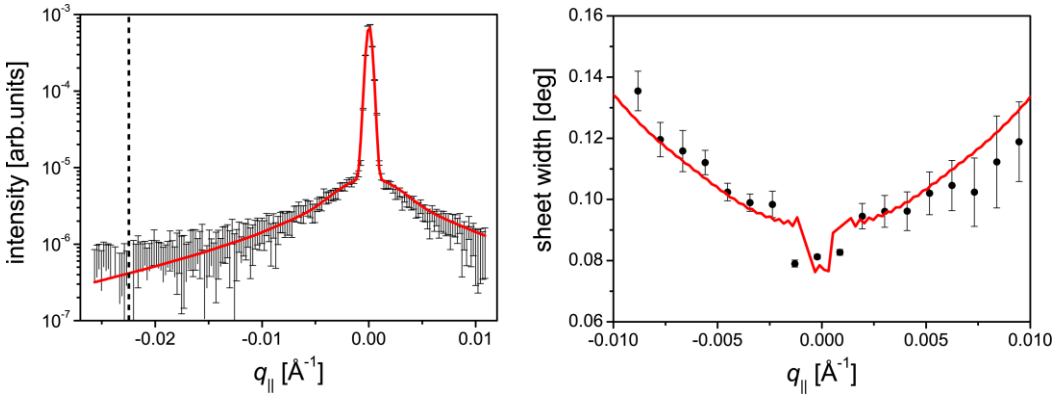

Figure S1: Measured (data points) and simulated (solid line) second Bragg sheets of DPPC membrane multilayers at 60 °C and $h_{rel} \approx 95$ %. Left column: Intensity integrated along Γ plotted as a function of $q_{||}$. The vertical dashed line indicates the position of the sample horizon. Right column: width of the sheet along Γ plotted as a function of $q_{||}$.

Fig. S1 shows the integrated intensity (left) and the width (right) of the second Bragg sheet measured from chain-deuterated DPPC membrane multilayers at 60 °C and 95 % relative humidity (H_2O vapor), where the multilayers exhibit a lamellar periodicity of d = 50.9 Å. The modeled signals (solid red lines) corresponding to the best matching parameters are superimposed on the experimental data points. The best matching model parameters are summarized in Table S1. The bending rigidity could not be extracted from neutron scattering experiments at full hydration, since the second Bragg sheet is suppressed by a form factor minimum at this condition. Instead, data recorded at a controlled relative humidity was analyzed.

System	η	λ [Å]	R [µm]	κ [k_BT]	B [MPa]
DPPC-D	0.010±0.001	6±1	0.5±0.1	18±3	46±7

Table S1: Parameters of the best matching model for DPPC membrane multilayers at T = 60 °C and $h_{rel} \approx 95$ %.

Off-Specular Neutron Scattering Intensity from Interacting DPPC Membranes Doped with 25 mol% Le^X Lipid with and without 5 mM Ca^{2+}

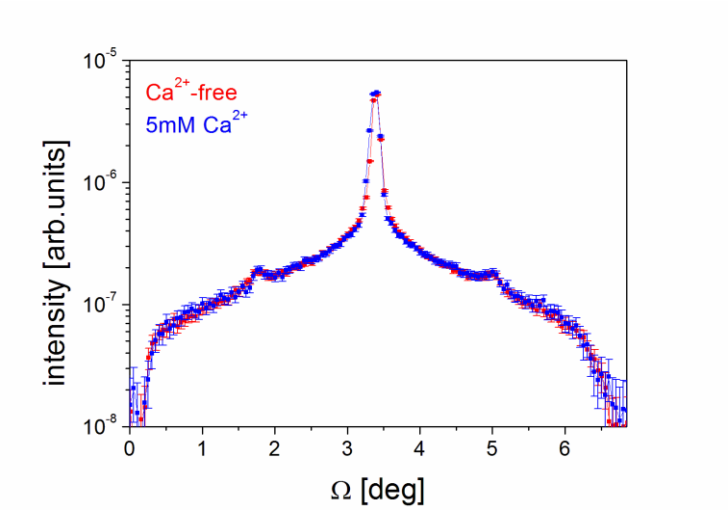

Figure S2: Γ-integrated intensities of the second Bragg sheets of DPPC membrane multilayers doped with 25 mol% Le^X lipid at 60 °C measured in the absence (red) and in the presence (blue) of 5 mM Ca^{2+}. The signals are identical within the experimental error.

Electrostatic Pressure between two Charged Surfaces in Electrolytes

Text S2: The electric potential $\psi(x)$ between the two charged surfaces in the mixed electrolyte was calculated by numerically integrating the Poisson-Boltzmann equation.

$$\frac{d^2\psi}{dx^2} = -\frac{\rho}{\varepsilon\varepsilon_0} = -\frac{1}{\varepsilon\varepsilon_0}\sum_m z_m e\rho_{0m}\exp\left(-z_m e\psi/k_B T\right),$$

with two boundary conditions(1) that depend on d_W:

1) $$\left.\frac{d\psi}{dx}\right|_{x=0} = 0$$

2) $$\left.\frac{d\psi}{dx}\right|_{x=d_W/2} = -\frac{\sigma}{\varepsilon\varepsilon_0}$$

Here, $k_B T$ denotes the thermal energy, ε_0 the permittivity of vacuum, ε the relative dielectric constant, ρ_{0m} and z_m the bulk density and charge number of ion species *m*, and *e* the elementary charge. *x* = 0 coincides with the "midplane" (i.e. the center between the two charged surfaces). Boundary condition 1 accounts for the symmetry requirement, while boundary condition 2 accounts for the potential gradient at the surfaces, which is proportional to their charge density σ. This boundary value problem was solved numerically using a finite difference technique with Richardson extrapolation. The repulsive interaction Π_{ES} of the two charged surfaces across the electrolyte is then given by(2):

$$\Pi_{ES} = k_B T\sum_i \rho_{0,i}\left(\exp\left(-z_i e\psi_{mp}/k_B T\right)-1\right).$$

This indicates that the electrostatic repulsion can be expressed with the osmotic pressure created by the ion enrichment at the midplane, which is determined by the midplane potential ψ_{mp}. To compute the electrostatic repulsion as a function of the separation distance, ψ_{mp} was calculated as a function of d_W.

1. Ninham, B. W., and V. A. Parsegian. 1971. Electrostatic Potential between Surfaces Bearing Ionizable Groups in Ionic Equilibrium with Physiologic Saline Solution. J. theor. Biol. 31:405-428.
2. Israelachvili, J. N. 1991. Intermolecular and Surface Forces. Academic Press Inc., London.

Reciprocal Space Coordinates of Double Scattering Peaks

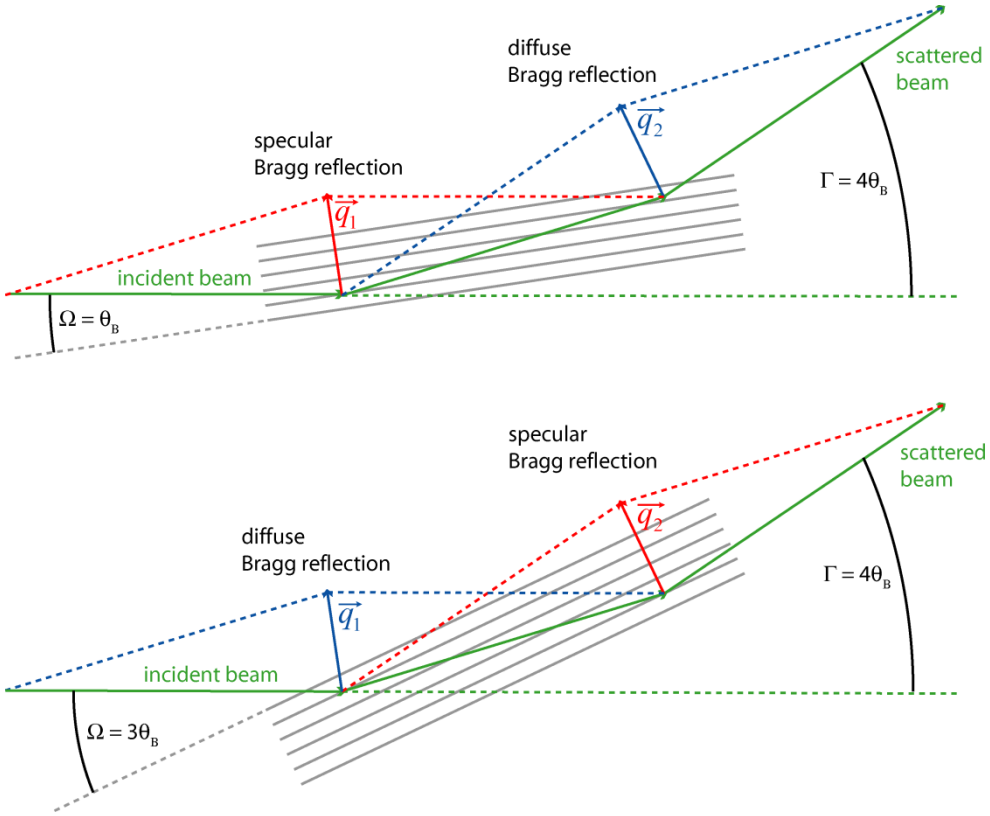

Fig. S3: Geometrical description of double scattering in multilayer systems. θ_B denotes the Bragg angle of the multilayers. (top) specular Bragg reflection ($\vec{q}_1$) followed by diffuse Bragg reflection ($\vec{q}_2$). A peak is observed at $\Omega = \theta_B$ and $\Gamma = 4\theta_B$. (bottom) diffuse Bragg reflection ($\vec{q}_1$) followed by specular Bragg reflection ($\vec{q}_2$). A peak is observed at $\Omega = 3\theta_B$ and $\Gamma = 4\theta_B$.

Text S3: Let the angle of incidence Ω, at which a beam impinges to a set of oriented rough multilayers, coincide with the first order Bragg angle $\theta_B = \arcsin(\lambda/2d)$. This scenario is depicted in Fig. S3 (top). The specularly reflected beam with the intensity $S(\Gamma = 2\theta_B, \Omega = \theta_B)$ may be scattered for a second time in a diffuse manner. The angle of incidence for this second process is $-\theta_B$, as determined by the preceding specular Bragg reflection. Under this condition the scattering function $S(\Gamma, \Omega = -\theta_B)$ possesses an intensity peak for $\Gamma = 2\theta_B$, and therefore the intensity of this secondary scattering process is proportional to $S(\Omega = -\theta_B, \Gamma = 2\theta_B)$. The resulting scattering angle (i.e., the detection angle Γ) for this double scattering process is $\Gamma = 4\theta_B$, as shown in the figure. Thus, a peak in the double scattering intensity I_{DS} is found for $\Omega = \theta_B$ and $\Gamma = 4\theta_B$, with:

$$I_{DS}(\Omega = \theta_B, \Gamma = 4\theta_B) \propto S(\Omega = \theta_B, \Gamma = 2\theta_B) \cdot S(\Omega = -\theta_B, \Gamma = 2\theta_B)$$

This peak represents a specular first order Bragg reflection followed by a diffuse first order Bragg reflection. An analogous double scattering process is depicted in the same figure (bottom) and represents the reverse sequence of single scattering processes, with the intensity:

$$I_{DS}(\Omega = 3\theta_B, \Gamma = 4\theta_B) \propto S(\Omega = 3\theta_B, \Gamma = 2\theta_B) \cdot S(\Omega = \theta_B, \Gamma = 2\theta_B)$$

For reason of symmetry:

$$I_{DS}(\Omega = \theta_B, \Gamma = 4\theta_B) = I_{DS}(\Omega = 3\theta_B, \Gamma = 4\theta_B)$$

The corresponding double scattering peaks are found at the following reciprocal space coordinates:

$$q_z = \frac{2\pi}{\lambda}(\sin\theta_B + \sin 3\theta_B) \cong \frac{4\pi}{d},\ q_{\parallel} = \pm\frac{2\pi}{\lambda}(\cos\theta_B - \cos 3\theta_B) \cong \pm\frac{2\pi}{\lambda}\left(\frac{\lambda}{d}\right)^2$$